BIOMOLECULES & THERAPEUTICS

Original Article
Biomol Ther 27(4), 386-394 (2019)

Inhibition of ER Stress by 2-Aminopurine Treatment Modulates Cardiomyopathy in a Murine Chronic Chagas Disease Model

Janeesh Plakkal Ayyappan[1], Kezia Iizardo[1], Sean Wang[2], Edward Yurkow[2] and Jyothi F Nagajyothi[1,*]

[1]*Department of Microbiology, Biochemistry and Molecular Genetics, Public Health Research Institute, New Jersey Medical School, Newark, NJ 07103,*
[2]*Rutgers Molecular Imaging Center, Piscataway, NJ 08854, USA*

Abstract

Trypanosoma cruzi infection results in debilitating cardiomyopathy, which is a major cause of mortality and morbidity in the endemic regions of Chagas disease (CD). The pathogenesis of Chagasic cardiomyopathy (CCM) has been intensely studied as a chronic inflammatory disease until recent observations reporting the role of cardio-metabolic dysfunctions. In particular, we demonstrated accumulation of lipid droplets and impaired cardiac lipid metabolism in the hearts of cardiomyopathic mice and patients, and their association with impaired mitochondrial functions and endoplasmic reticulum (ER) stress in CD mice. In the present study, we examined whether treating infected mice with an ER stress inhibitor can modify the pathogenesis of cardiomyopathy during chronic stages of infection. *T. cruzi* infected mice were treated with an ER stress inhibitor 2-Aminopurine (2AP) during the indeterminate stage and evaluated for cardiac pathophysiology during the subsequent chronic stage. Our study demonstrates that inhibition of ER stress improves cardiac pathology caused by *T. cruzi* infection by reducing ER stress and downstream signaling of phosphorylated eukaryotic initiation factor (P-eIF2α) in the hearts of chronically infected mice. Importantly, cardiac ultrasound imaging showed amelioration of ventricular enlargement, suggesting that inhibition of ER stress may be a valuable strategy to combat the progression of cardiomyopathy in Chagas patients.

Key Words: Chagas disease, Cardiomyopathy, Mitochondrial stress, Endoplasmic reticulum stress, 2-Aminopurine

INTRODUCTION

Chagas disease (CD), caused by parasite *Trypanosoma cruzi*, is endemic in Latin America, where it is responsible for 12,000 deaths per year. CD has two main stages in patients – acute and chronic (Tanowitz *et al*.,1992). Acute infection causes mild symptoms, and mortality (approximately 5%) is reported predominantly in untreated children (Memorial, 2009). However, chronic Chagas disease, which is typically asymptomatic, may progress to the chronic cardiac form in approximately 30% of *T. cruzi* infected people (Nunes *et al*., 2013). The severity and manifestations of cardiac symptoms vary in these patients and can lead to death due to cardiomyopathy, arrhythmias and/or progressive heart failure (Quijano-Hernandez and Dumonteil, 2011). The mechanism(s) underlying the transition between asymptomatic and cardiac form is not completely understood. Furthermore, there are no efficient drugs or vaccines to prevent the pathogenesis of Chagasic cardiomyopathy (Jelicks and Tanowitz, 2011).

Murine CD models are suitable to investigate the pathogenesis of cardiomyopathy because they recapitulate the cardiac symptoms of Chagas patients (Machado *et al*., 2012; Nagajyothi *et al*., 2014). Acute and chronic stages of CD can be modeled in mice by manipulating the strain and number of *T. cruzi* parasites used in infection, and mouse diet (Soares *et al*., 2010; Kezia *et al*., 2018). For example, we have demonstrated that infecting Swiss mice with 10^3 trypomastigotes of *T. cruzi* (Brazil strain) leads to acute infection with low mortality rate and parasitemia before 35 days post infection (DPI) and chronic cardiomyopathy after approximately 90 DPI (Jelicks *et al*., 2002; Johndrow *et al*., 2014). Between 35 and 90 DPI, these infected mice usually appear to be in the indeterminate (asymptomatic) stage, showing no significant change in serum inflammatory markers and parasitemia. Thus, these models of CD are suitable to investigate the molecular mechanism(s) of the pathogenesis of cardiomyopathy.

Open Access **https://doi.org/10.4062/biomolther.2018.193**

Received Oct 2, 2018 **Revised** Jan 17, 2019 **Accepted** Jan 25, 2019
Published Online Mar 13, 2019

***Corresponding Author**
E-mail: jfn31@njms.rutgers.edu
Tel: +1-973-854-3450, Fax: +1-973-854-3101

Table 1. A list of genes and their mouse-specific primer sequences used for real-time PCR

Primer name	Forward (5′-3′)	Reverse (3′-5′)	Accession number
BIP	GGTGCAGCAGGACATCAAGTT	CCACCTCCAATATCAACTTGA	NC_000068.7
TNF-A	CCCTCACACTCAGATCATCTTCT	GCTACGACGTGGGCTACAG	NC_000083.6
COX3	CCTTCGACCTGACAGAAGGA	GATGCTCGGATCCATAGGAA	NC_005089.1
CAT	ACCCTCTTATACCAGTTGGC	GCATGCACATGGGGCCATCA	NM_009804.2
CYTB	ATTCCTTCATGTCGGACGAG	ACTGAGAAGCCCCCTCAAAT	X57779.1
GPX1	ACAGTCCACCGTGTATGCCTTC	CTCTTCATTCTTGCCATTCTCCTG	NM_008160.6
ATP6	CCTTCCACAAGGAACTCCA	GGTAGCTGTTGGTGGGCTAAA	NC_005089
GPX2	GAAAGACAAGCTGCCCTACC	TCCATATGATGAGCTTGGGA	NM_030677.2
ND1	CTGGCTACTGCGTACATCCA	TCTCCAAACCCTTTGACACA	NC_000086.7
MNSOD	CACATTAACGCGCAGATCATG	CCAGAGCCTCGTGGTACTTCTC	NM_013671.3
PGC1α	AACCACACCCACAGGATCAGA	TCTTCGCTTTATTGCTCCATGA	NR_132764.1
GSK3 BETA	CAGTGGTGTGGATCAGTTGG	ATGTGCACAAGCTTCCAGTG	NM_019827.6
COL1	GAGCGGAGAGTACTGGATCG	GCTTCTTTTCCTTGGGGTTC	BC050014
COLIII	GCACAGCAGTCCAACGTAGA	TCTCCAAATGGGATCTCTGG	BC058724
SERCA2	CTGTGGAGACCCTTGGTTGT	CAGAGCACAGATGGTGGCTA	NR_027838.1
PERK	GATGACTGCAATTACGCTATCAAG	CCTTCTCCCGTGCCAACTC	NC_000072.6
Erol-Alfa	GCATTGAAGAAGGTGAGCAA	ATCATGCTTGGTCCACTGAA	NC_000080.6
ATF4	ATGGCCGGCTATGGATGAT	CGAAGTCAAACTCTTTCAGATCCATT	NM_009716.3
GADD34	CCCGAGATTCCTCTAAAAGC	CCAGACAGCAAGGAAATGG	U83984.1
BCL2	ACTTCGCAGAGATGTCCAGTCA	TGGCAAAGCGTCCCCTC	NM_009741.5
BCL-XL	GTAAACTGGGGTCGCATTGT	TGGATCCAAGGCTCTAGGTG	L35049.1
TNFRSF1A	CATCCCCAAGCAAGAGTCATG	GCTACAGACGTTCACGATGC	NM_011609.4
BAK	CCTGAAACCTTGGCCCCT	AGCCGTGCAAAGACGAAGAC	NC_000083.6
CHOP	CTGCCTTTCACCTTGGAGAC	CGTTTCCTGGGGATGAGATA	NC_000076.6
HPRT	GTTGGATCAAGGCCAGACTTTGTT	GAGGGTAGGCTGGCCTATAGGCT	NC_000086.7

Earlier, using these murine CD models, we demonstrated that *T. cruzi* infection induces cardiac lipid accumulation, which causes oxidative stress and inflammation, leading to cardiomyopathy during the chronic stage of infection (Jelicks *et al*., 2002; Zhou *et al*., 2013). Others have reported that cardiac inflammation, apoptosis and fibrosis are the major causes of chagasic cardiomyopathy (Tostes *et al*., 2005). Therefore, it is of utmost interest to understand the precise regulatory mechanisms that regulate inflammation, mitochondrial stress and apoptosis in the cardiac pathogenesis of CD. Endoplasmic reticulum (ER) is a cellular organelle important for regulating calcium homeostasis, lipid metabolism, protein synthesis, and posttranslational modification and trafficking, and disturbance of ER homeostasis triggers the ER stress response and induces apoptotic cell death (Malhotra and Kaufman, 2007; Jacquemyn *et al*., 2017). One demonstrated cause of ER stress is the accumulation of intracellular lipids (Volmer and Ron, 2015). Previously we demonstrated cardiac lipid accumulation in *T. cruzi* infected mice (Jelicks *et al*., 2002; Zhou *et al*., 2013), suggesting that ER stress may be part of the mechanism leading to cardiac dysfunction during CD. In the present study, we investigated the role of ER stress in causing cardiac inflammation, mitochondrial dysfunction, apoptosis, fibrosis and cardiomyopathy in a *T. cruzi* infected murine chronic CD model. We also demonstrated that infected mice treated with an ER stress inhibitor, 2-Aminopurine (2AP), during indeterminate stage (after 40 DPI) significantly modifies cardiac dysfunction, including cardiomyopathy caused by chronic *T. cruzi* infection. The results shed light on the role of cardiac ER stress in the pathogenesis of Chagasic cardiomyopathy and suggest that developing drugs that inhibit cardiac ER stress may be a valuable strategy to combat cardiac pathology in chronic Chagas disease.

MATERIALS AND METHODS

Animal model and experimental design

Trypomastigotes of *T. cruzi* Brazil strain was propagated in a myoblast line (L6E9) and maintained by serial passage in C3H mice (Jackson Laboratories, Bar Harbor, ME, USA) as previously described (Combs *et al*., 2005). *T. cruzi* (epimastigote DNA) was first analyzed by PCR targeted to sequences of their kDNA minicircles using the *T. cruzi* 195-bp repeat DNA-specific primers TCZ-F (5′-GCTCTTGCCCACAAGGGTGC- 3′) and TCZ-R (5′-CCAAGCAGCGGATAGTTCAGG-3′) as demonstrated earlier (Combs *et al*., 2005). Thereafter, a PCR assay based on the non-transcribed spacer of the miniexon gene was performed to characterize the strain (Brazil strain DTU1, 21; Minning *et al*., 2011) using the primer set specific to Tc1 5′-ACACTTTCTGTGGCGCTGATCG and Me: 5′-TACCAATATAGTACAGAAACTG as described earlier (Fernandas *et al*., 2001).

Swiss (male CD-1® IGS, Jackson Laboratories) mice were maintained on a 12-h light/dark cycle. A group of mice (n=55) were infected intraperitoneally (i.p., n=35) at 6-8 weeks of age with 10^3 trypomastigotes of the Brazil strain and fed on Formulab diet #5008 (Lab diet). After 40 days post infection (DPI), both uninfected and infected mice were divided into two groups and one group gavaged with 2-Aminopurine (100 mg/kg body weight) and the other with vehicle alone for 80 days (120 DPI) (Supplementary Fig. 3). The dose of 2-Aminopurine

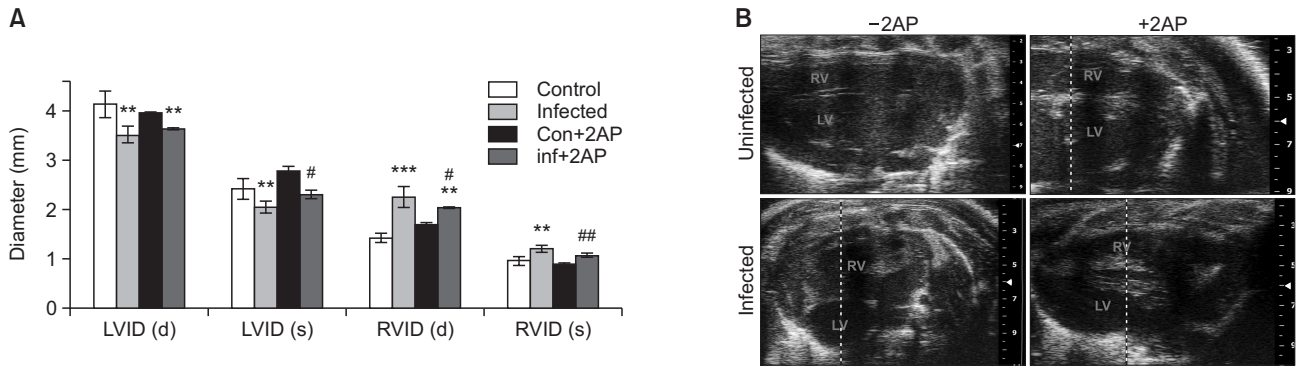

Fig. 1. Treatment with 2AP during indeterminate stage improved the morphology of the heart during murine chronic CD at 100 DPI (n=5/group). (A) A bar graph representing the ultrasound analysis of the hearts at 100 DPI. Ultrasound analysis of the hearts both at diastole (d) and systole (s) condition showed a significant decrease in the left ventricle internal diameter (LVID) and significant increase in the right ventricle internal diameter (RVID) in the infected mice compared to uninfected mice at 100 DPI. However, the infected mice treated with 2AP displayed significantly modified LVID (s) and RVID (both d and s) compared to infected untreated mice at 100 DPI. (B) Representative cardiac ultrasound images of mice (uninfected, infected, uninfected+2AP treated and infected 2AP treated). Statistical significance compared to uninfected untreated mice and infected untreated mice are represented by $^{**}p \leq 0.01$, $^{***}p \leq 0.001$, and $^{\#}p \leq 0.05$ or $^{\#\#}p \leq 0.01$, respectively.

was selected based on the published data (Zhou *et al*., 2013, where they have used 200 mg/kg body weight for alternative days) to alleviate ER stress in mice, and the treatment continued till mice reached 120 DPI (euthanized at this time point to collect tissue samples for analysis). Cardiac imaging analysis was done at 100 DPI and all the animals were sacrificed at 120 DPI to collect heart and blood samples for the following studies. All animal experimental protocols were approved by the Institutional Animal Care and Use and Institutional Biosafety Committees of Rutgers University and adhere to the National Research Council guidelines.

Cardiac ultrasound imaging analysis

The cardiac ultrasound imaging of the mice were performed at 100 DPI (chronic stage of infection) using a Vevo®2100 ultra-high frequency ultrasound system (Visual Sonics Inc., Toronto, Canada) at the Rutgers University Molecular Imaging Center. This system is used routinely to conduct rodent echocardiography consisting of standard and advanced endpoints of heart and vessel morphology, as well as functional endpoints that include cardiac output, stroke volume, fractional shortening and changes in myocardial and ventricular volume occurring during diastole and systole. Doppler ultrasound capabilities of the system is also used to determine the blood flow velocities of the aorta and pulmonary arteries as well as to profile mitral valve function. All imaging procedures were performed under inhalation anesthesia with isoflurane at a concentration of 4-5% for induction and 1-2% for maintenance. Scan time was approximately 1 h/mouse. Prior to evaluation, the hair was removed from the skin of the chest area using a depilatory agent and the anesthetized mouse was mounted in the supine position on the heated stage equipped with an anesthesia nose cone. Conductive electrolyte gel was applied to the ECG electrodes and the paws of the mouse were affixed to the electrodes using surgical tape. The body temperature was continuously monitored via a temperature probe and physiological stability was visually controlled by the periodic adjustment of the anesthesia delivery rate. For scanning, ultrasound gel was applied to the chest area of the mouse and the ultrasound transducer (MS-550D, 22-55MHz, Fujifilm Visualsonics, Toronto, ON, Canada) was mounted on the imaging station and position over the heart, which is tilted to position the ultrasound transducer on the right lateral surface of the rib cage. Fine adjustments are made to the position of the transducer that is mounted in a mechanized transducer clamp with x, y, z-positioning knobs/wheels. Based on real-time sonogram videos, further adjustments are made to the stage and knobs to optimize the visualization of the right and left ventricles. When optimal positioning is achieved, a cine movie displaying the beating heart is captured in M-mode and stored. At a later time the movie is viewed and still frames of the movie are used to make specific measurements in systole and diastole. In some cases, both right and left ventricles cannot be optimally visualized at a single position. In those cases additional images are captured and optimal measurements are determined in separate images. When the scans were completed, the animals were monitored and allowed to recover under a heat lamp or heat pad. B-mode, M-mode and Pulse Wave Doppler image files were collected from both the parasternal long axis and short axis views. Morphometric measurements and blood flow velocity of major vessels and valves were determined using image analysis tools available in the Vevo® workstation software (Fujifilm Visualsonics).

Immunoblot analysis

Heart lysates were prepared as previously described (Nagajyothi *et al*., 2014). An aliquot of each sample (30 μg protein) was subjected to SDS-PAGE and the proteins were transferred to nitrocellulose filters for immunoblot analysis. BIP- specific rabbit monoclonal antibody (1:1000 dilution, C50B12, Cell Signaling Technology, Danvers, MA, USA), TNF-alpha-specific rabbit polyclonal antibody (1:2000 dilution, AB6671, Abcam, Cambridge, MA, USA). HSP60 specific rabbit monoclonal antibody (1:1000 dilution, 12165, Cell Signaling), Phospho-eIF2α (Ser51) specific rabbit monoclonal antibody 1:1000 dilution, 3597, Cell Signaling) and CHOP-specific mouse monoclonal antibody (1:1000 dilution, L63F7, Cell Signaling), were used as primary antibody. Horseradish peroxidase-conjugated goat anti-mouse immunoglobulin (1:2000 dilution, Thermo Scientific, Springfield Township, NJ, USA) or

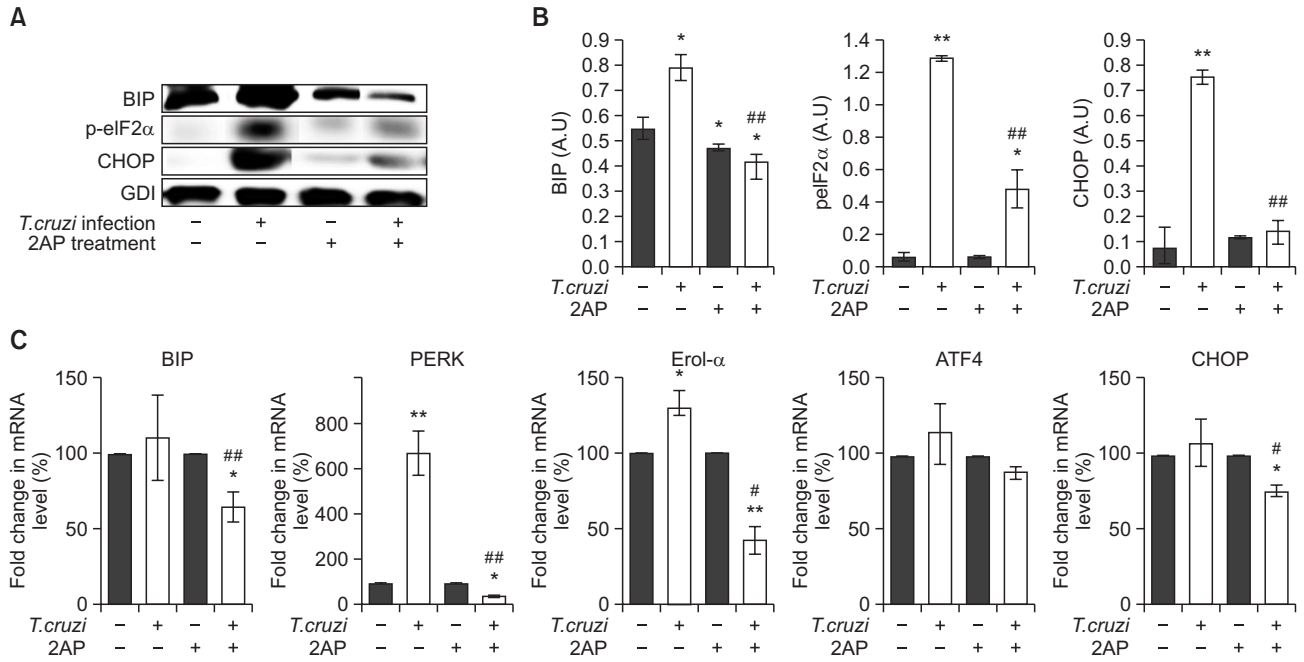

Fig. 2. 2AP inhibits cardiac ER stress in chronic CD mice (n=10/group). (A) Immunoblot analysis demonstrated a significant decrease in the levels of ER stress markers BIP, p-eIF2α and CHOP in the hearts of infected mice treated with 2AP compared to infected untreated mice at 120 DPI. (B) Fold changes in the protein levels of BIP, pELF2α and CHOP were normalized to guanosine nucleotide dissociation inhibitor (GDI) expression and represented as the bar graph. (C) qPCR analysis demonstrated a significant decrease in the mRNA levels of ER stress response genes such as BIP, PERK, Erol-α, ATF4 and CHOP in the hearts of infected mice treated with 2AP compared to infected untreated mice at 120 DPI. Statistical significance compared to uninfected untreated mice and infected untreated mice are represented by **p*≤0.05, ***p*≤0.001, and #*p*≤0.05 or ##*p*≤0.01, respectively.

horseradish peroxidase-conjugated goat anti-rabbit immunoglobulin (1:2000 dilution, Thermo Scientific) were used to detect specific protein bands (explained in figure legends) using a chemiluminescence system BioRad (Combs *et al*., 2005). Guanosine nucleotide dissociation inhibitor (GDI) (1:10,000 dilution, 71-0300, and rabbit polyclonal, Invitrogen, CA, USA) and a secondary antibody horseradish peroxidase conjugated goat anti-rabbit (1:2000 dilution, Amersham Biosciences, Little Chalfont, UK) was used to normalize protein loading.

Real time PCR quantification

Total host RNA from the heart of *T.cruzi* infected mice and matched uninfected control animals at 120 DPI was isolated, using the Trizol reagent (Invitrogen). Isolated RNA was purified by on-column digestion of the contaminating DNA using DNase I. The quality and quantity of the purified RNA were assessed by a NanoDrop instrument (NanoDrop Products, Wilmington, DE, USA), as previously described (Nagajyothi *et al*., 2014). RNA was reverse transcribed from 100 ng of total RNA using All-in-One cDNA Synthesis SuperMix (Biotools, Madrid, Spain) according to the manufacturer's protocol. The primers used for the amplification of quantitative PCR (qPCR) of BIP, TNF-A, COX3, CYTB, ATP6, ND1, MNSOD, Catalase (CAT), (GPX1, GPX2, PGC1α, GSK3 BETA, collagen isoform 1 (COL1), collagen isoform 3 (COLIII), SERCA2, PERK, Erol-α, ATF4, GADD34, BCL2, BCL-XL, TNF-R1, BAK, CHOP and HPRT (Hypoxanthine-guanine phosphoribosyltransferase) genes (Table 1). The qPCR was run using Power SYBR™ Green PCR Master Mix (Thermo Scientific) following the manufacturer's protocol. To normalize gene expression and to calculate fold change mRNA expression of the housekeeping gene, HPRT was measured. For each sample, both the housekeeping and target genes were amplified in triplicate using the reaction condition and analytic parameters.

Immunohistochemical analyses

Freshly isolated tissues were fixed with phosphate-buffered formalin overnight and then embedded in paraffin wax. Hematoxylin and eosin (H&E) staining was performed, and the images were captured as previously published (Nagajyothi *et al*., 2014). Immunohistochemical analysis was performed on the formalin-fixed heart using BIP- specific rabbit monoclonal antibody 1:500 dilution, C50B12, Cell Signaling), Phospho-eIF2α (Ser51) specific rabbit monoclonal antibody 1:500 dilution, 3597, Cell Signaling) and CHOP-specific mouse monoclonal antibody (1:1000 dilution, L63F7, Cell Signaling) as demonstrated earlier (Nagajyothi *et al*., 2014).

Statistical analysis

Statistical analyses were performed using a Student's *t*-test as appropriate and significance differences were determined as *p*-values between <0.05 and <0.001 as appropriate.

RESULTS

2AP treatment significantly diminishes ventricular dilation caused by *T. cruzi* infection

Previously we demonstrated significant alterations in cardiac morphology in *T. cruzi* infected mice during the chronic

phase of infection, including a reduction in the left ventricle internal diameter (LVID) and an increase in the right ventricle internal diameter (RVID) (at both diastole and systole) (Jelicks and Tanowitz, 2011). Here we evaluated whether inhibiting cardiac ER stress by treating infected mice with 2AP modulates *T. cruzi* infection caused LVID reduction and RVID dilation using a Visual Sonics, Vevo2100 ultra-high frequency ultrasound system. As previously demonstrated (Jelicks *et al*., 2002; Soares *et al*., 2010), *T. cruzi* infected mice showed significantly reduced LVID and dilated RVID (measured at both systolic and diastolic phase) at 100 DPI (Fig. 1A, 1B). In contrast, 2AP treated infected mice showed significantly ameliorated LVID (systole) and RVID (both diastole and systole) compared to infected untreated mice (Fig. 1A, 1B). Doppler flow profiles demonstrated a significant difference ($p \leq 0.01$) in the ejection fractions (%) between different groups; uninfected mice (EF%- 59 ± 2), infected mice (EF%- 48 ± 2.8), 2AP treated uninfected mice (EF%- 60 ± 5.2) and 2AP treated infected mice (EF%- 54 ± 3.1). However, we did not detect any significant difference in fractional shortening measurements (data not shown). These data demonstrated that inhibition of cardiac ER stress improves cardiac morphology in chronic *T. cruzi* infection.

2AP treatment during indeterminate stage reduces cardiac ER stress in chronic Chagas mice

Immunoblot analyses demonstrated significantly increased levels of cardiac ER stress markers such as BIP (Immunoglobulin Binding Protein), p-eIF2α (phosphorylated eukaryotic translation initiation factor 2 alpha), and CHOP (C/EBP homologous protein) in chronic *T. cruzi* infected mice compared to uninfected mice (Fig. 2A, 2B). Treating infected mice with 2AP, an ER stress inhibitor, resulted in a significant reduction in the levels of cardiac ER stress markers (Fig. 2A, 2B). Immunohistochemical analyses of cardiac sections also demonstrated a significant decrease in the levels of BIP, p-eIF2α and CHOP in infected 2AP treated mice compared to untreated mice (Supplementary Fig. 1). Next, qPCR analysis was performed to analyze the effect of 2AP treatment on the mRNA levels of several genes involved in response to ER stress (Fig. 2C). We observed a significant decrease in the levels of BIP ($p<0.05$), PRKR-like endoplasmic reticulum kinase (PERK) ($p<0.001$), ER-residing protein endoplasmic oxidoreductin-1 alfa (Erol-α), ($p<0.05$), and CHOP($p<0.05$) in the hearts of infected 2AP treated mice compared to infected untreated mice (Fig. 2C). These data demonstrate that 2AP acts as a potent ER stress inhibitor and reduces cardiac ER stress in chronic *T. cruzi* infected mice.

Reducing cardiac ER stress results in decreased apoptotic signals during chronic infection

Irreversible ER stress induces several pro-apoptotic mechanisms to eliminate damaged cells (Weber and Menko, 2005). ER stress-mediated cell death is executed by the canonical mitochondrial apoptosis pathway, where the BCL-2 (B-cell lymphoma/leukemia-2) family plays a crucial role (Carpio *et al*., 2015). Transcriptional and post-transcriptional mechanisms are activated to regulate pro-apoptotic members of the BCL-2 family that facilitate cytochrome c release from the mitochondria and calcium release from the ER to engage downstream apoptotic signaling events (Feng *et al*., 2010). Our qPCR analysis demonstrated a significant increase in the cardiac mRNA

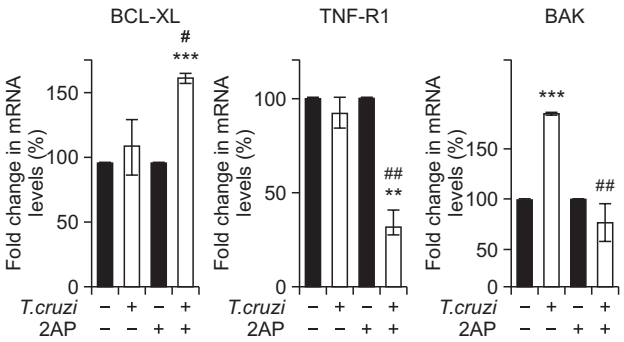

Fig. 3. Treatment with 2AP during indeterminate stage decreased apoptotic signaling in chronic *T. cruzi* infected mice (n=10/group). qPCR analysis demonstrated a significant increase in the cardiac mRNA levels of anti-apoptotic BCL-Xl, and significant decrease in mRNA levels of pro-apoptotic markers TNF-R1 and BAK in the hearts of infected mice treated with 2AP compared to infected untreated mice at 120 DPI. Statistical significance compared to uninfected untreated mice and infected untreated mice are represented by $^{**}p \leq 0.01$, $^{***}p \leq 0.001$, and $^{\#}p \leq 0.05$ or $^{\#\#}p \leq 0.01$, respectively.

levels of B-cell lymphoma-extra-large (BCL-Xl) ($p<0.05$) and decrease in Tumor necrosis factor receptor 1 (TNF-R1) ($p<0.01$) and BCL2 Antagonist/Killer 1 (BAK) ($p<0.01$) levels in infected 2AP treated mice compared to infected untreated mice (Fig. 3). BCL-X1 is an anti-apoptotic marker, while TNF-R1 and BAK are known apoptotic markers (Westphal *et al*., 2011; Cao and Kaufman, 2014). These data indicate that 2AP induced inhibition of ER stress decreased the expression of pro-apoptotic markers in the hearts of infected mice during chronic infection.

2AP improves mitochondrial function and reduces oxidative stress in the hearts of *T. cruzi* infected mice

ER stress and mitochondrial oxidative stress regulate each other and form a vicious cycle, resulting in apoptosis (Li *et al*., 2016). To evaluate the effect of reduced ER stress on the cardiac mitochondrial function and oxidative stress, we measured mRNA levels of the genes involved in mitochondrial function: cytochrome c oxidase subunit 3 (COX3), cytochrome b (CYTB), ATP synthase Fo subunit 6 (ATP6) and NADH dehydrogenase, subunit 1 (ND1). We also measured the expression of anti-oxidative stress genes: mitochondrial antioxidant manganese superoxide dismutase (MNSOD), catalase (CAT), glutathione peroxidase 1 (GPX1), glutathione peroxidase 2 (GPX2), peroxisome proliferator-activated receptor γ coactivator 1 alfa (PGC1α) and glycogen synthase kinase 3 beta (GSK3β) in the heart samples of mice from different experimental groups (Fig. 4). This qPCR analysis demonstrated a significant decrease in the mRNA levels of some of the genes involved in mitochondrial function and oxidative stress resistance in the hearts of infected mice compared to uninfected mice (Fig. 4A, 4B). Furthermore, 2AP treatment significantly increased mRNA levels of the genes involved in mitochondrial function and resistance to oxidative stress in the hearts of infected mice compared to infected untreated mice (Fig. 4A, 4B).

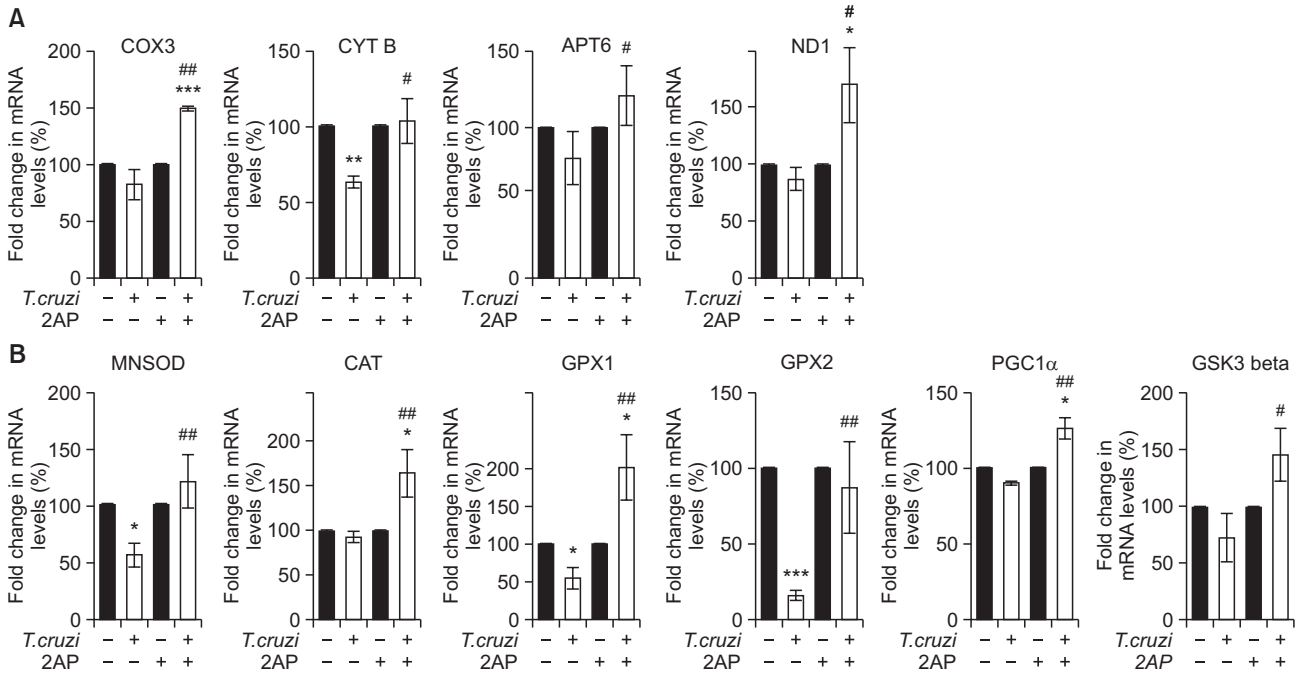

Fig. 4. Inhibition of cardiac ER stress by 2AP modified mitochondrial function by upregulating anti-oxidant genes during chronic *T. cruzi* infection (n=10). (A) qPCR analysis demonstrated a significant increase in the cardiac mRNA levels of genes involved in mitochondrial functions such as COX3, CYTB, ATP6 and ND1in infected mice treated with 2AP compared to infected untreated mice at 120 DPI. (B) 2AP treatment significantly upregulates mRNA levels of anti-oxidant genes such as MNSOD, CAT, GPX1, GPX2, PGC1α and GSK3 in the hearts of infected mice treated with 2AP compared to infected untreated mice at 120 DPI as demonstrated by qPCR analysis. Statistical significance compared to uninfected untreated mice and infected untreated mice are represented by *$p \leq 0.05$, ***$p \leq 0.001$, and $^{\#}p \leq 0.05$ or $^{\#\#}p \leq 0.01$, respectively.

Reduced ER stress significantly decreases cardiac inflammation

We have previously shown that *T. cruzi* infection induces increased infiltration of immune cells into the myocardium, leading to pro-inflammatory signaling (Jelicks *et al*., 2002; Soares *et al*., 2010). We used immunoblot analysis to quantify the levels of pro-inflammatory cytokine TNFα (tumor necrosis factor alpha) in the myocardium at 120 DPI. We found that cardiac TNFα levels significantly increased in infected mice compared to uninfected mice at 120 DPI (Fig. 5A, 5B). qPCR analysis also demonstrated a significant increase in TNF-alpha levels during infection compared to uninfected mice (Fig. 5C). However, the treatment with 2AP in infected mice significantly reduced the levels of TNFα in the hearts compared to untreated mice at 120 DPI (Fig. 5), indicating that reducing ER stress also counteracts the inflammatory processes in the heart.

Inhibition of ER stress modulates cardiac morphology in *T. cruzi* infected mice

Because the levels of TNFα in the hearts correlate with the levels of infiltrated immune cells into the myocardium during infection (Jelicks *et al*., 2002; Soares *et al*., 2010), we analyzed the levels of immune cells in the myocardium by histological analysis. Photomicrographs of H&E stained heart sections demonstrated significantly damaged cardiac morphology during *T. cruzi* infection compared to uninfected mice at 120 DPI. *T. cruzi* infection significantly increased the levels of infiltrated immune cells, lipid droplets, degenerating cardiac fibers and fibrosis in the hearts (Fig. 6, Supplementary Fig. 2). H&E stained cardiac sections of infected 2AP treated mice showed a significant decrease ($p \leq 0.01$) in cardiac damage (reflected by levels of infiltrated immune cells, lipid droplets, degenerating cardiac fibers, and cellular hypertrophy) compared to infected mice without treatment (Fig. 6A, Supplementary Fig. 2). We also observed significantly increased fibrosis and collagen deposition in the myocardium of infected mice compared to uninfected mice (Fig. 6B). However, infected mice treated with 2AP showed significantly reduced levels ($p \leq 0.01$) of fibrosis and collagen deposition in the heart sections compared to infected untreated mice (Fig. 6B). This observation was further confirmed by analyzing the mRNA levels of collagen I and III – genes whose overexpression results in collagen deposition (Van Kerckhoven *et al*., 2000) – in the heart samples (Fig. 6C). qPCR analysis demonstrated a significant increase in the cardiac mRNA levels of collagen I and III in the infected mice compared to uninfected mice. In contrast, the mRNA levels of collagen I and III in infected 2AP treated mice showed no significant difference compared to uninfected mice and were significantly reduced compared to infected untreated mice (Fig. 6C). These data demonstrate that 2AP treatment significantly improves cardiac morphology by reducing collagen deposition and fibrosis. Decreased cardiac collagen deposition improves contractile function of the myocardium deposition (Lipskaia *et al*., 2010). The cardiac isoform of the sarco/endoplasmic reticulum Ca2+ATPase (SERCA2a) plays a major role in controlling excitation/contraction coupling (Gupta *et al*., 2009). qPCR analysis demonstrated a significant increase in the mRNA levels of SARCA 2 in infected 2AP treated mice compared to

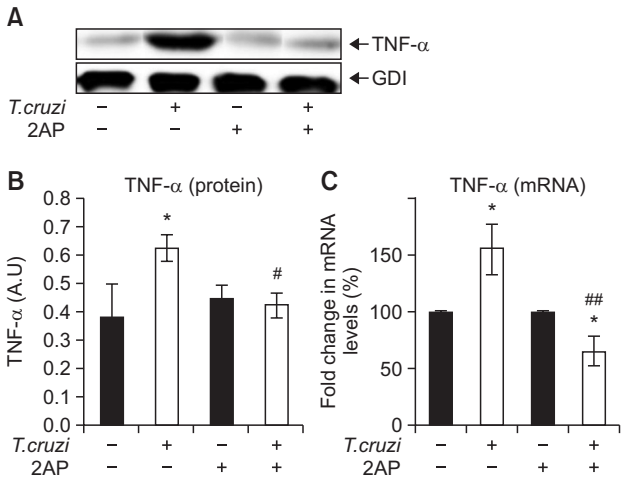

Fig. 5. Treatment with 2AP during the indeterminate stage reduced cardiac inflammation in chronic *T. cruzi* infected mice (n=10). (A) Immunoblot analysis demonstrated a significant decrease in the level of TNFα in the hearts of infected mice treated with 2AP compared to infected untreated mice at 120 DPI. (B) Fold changes in the protein levels of TNFα were normalized to GDI expression and represented as the bar graph. (C) qPCR analysis demonstrates a significant decrease in the mRNA levels of TNF-A in the hearts of infected mice treated with 2AP compared to infected untreated mice at 120 DPI. Statistical significance compared to uninfected untreated mice and infected untreated mice are represented by **p*≤0.05, ****p*≤0.001, and $^{\#}p$≤0.05 or $^{\#\#}p$≤0.01, respectively.

infected untreated mice (Fig. 6C). These data suggest that 2AP treatment decreases cardiac collagen deposition and improves cardiac contractile functions in infected mice.

DISCUSSION

We previously showed that acute *T. cruzi* infection in mice causes cardiac lipid accumulation, which in turn promotes mitochondrial oxidative stress and results in cardiac ventricular dilation and dysfunction (Garg *et al*., 2003; Han and Kaufman, 2016). Other studies have reported that intracellular lipid accumulation results in ER stress and cell death (Jacquemyn *et al*., 2017). In this study we tested the hypothesis that increased cardiac lipid accumulation may cause ER stress in the myocardium and form a vicious cycle with mitochondrial stress and exacerbate cardiac pathology during chronic infection. The most important findings of this report are (i) *T. cruzi* infection induces cardiac ER stress and results in ventricular dilation during chronic stages of infection, and (ii) oral feeding of the ER stress inhibitor 2AP to CD mice significantly reduced cardiac inflammation and pathology induced by chronic *T. cruzi* infection (Fig. 1, 6).

The ER is the main intracellular organelle in the secretory pathway as well as the site of biosynthesis for steroids, cholesterol, and other lipids (Malhotra and Kaufman, 2007). The main function of ER is to carry out appropriate protein folding, assembly, and disulfide bond formation, leading to production of functional, mature proteins in sacs called cisternae and the transport of synthesized proteins in vesicles to the Golgi apparatus. The accumulation of unfolded proteins in the lumen of ER causes ER stress characterized by increasing production of ER molecular chaperones and diminishing global protein synthesis, a process by which ER stress is relieved under physiological conditions (Volmer and Ron, 2015; Rozpedek *et al*., 2016). Activation of the signaling network in response to ER stress is known as unfolded protein response (UPR). Recent reports have demonstrated that lipids/lipoproteins can also trigger UPR (Gardner *et al*., 2013). The pathophysiological insults caused by acute *T. cruzi* infection lead to cardiac accumulation of lipids and unfolded proteins in the ER and result in ER stress. There are three distinct UPR signaling pathways triggered in response to ER stress, which are mediated by PERK, ATF6, and IRE1 (Harding *et al*., 2000). PERK is the major protein responsible for decreasing the mRNA translation under ER stress, inhibiting influx of newly synthesized proteins into the already stressed ER compartment (B'chir *et al*., 2013). This translational attenuation is mediated by phosphorylation of eIF2α. The phosphorylation of eIF2α (P-eIF2α) inhibits the recycling of eIF2α to its active GTP-bound form, which is required for the initiation phase of polypeptide chain synthesis. Paradoxically, eIF-2α phosphorylation also enhances the autophagy gene transcription signaling inducing cell death (Zhao and Ackerman, 2006). Thus, elevation of PERK- P-eIF2α signaling along with the other ER molecular chaperones inhibits global protein synthesis. However, constant inhibition of global protein synthesis might suppress normal cellular functions and cause cell death, and resulting in pathological conditions of the heart in Chagas disease.

Reminiscent of our previous studies, histological analysis of the hearts of chronic *T. cruzi* infected mice demonstrated significantly elevated lipid droplets and infiltrated immune cells (compared to uninfected mice), which could be the main cause of cardiac pathology in the infected mice. Increased cardiac lipid levels might lead to elevated UPR, causing ER stress (Gardner *et al*., 2013; Zhou *et al*., 2013). We found that the cardiac ER stress caused by *T. cruzi* infection upregulates BIP dissociation, resulting in high levels of PERK, phosphorylation of eIF2α, ATF4 and chaperone proteins (e.g., CHOP) in the hearts (Fig. 2). We showed myocardial inflammation, apoptosis and fibrosis in the hearts of chronic infected mice, as demonstrated by increased levels of TNFα, apoptotic markers (CHOP and BAK) and collagen levels in the hearts of infected mice at 120 DPI. These findings suggest that increased eIF-2α phosphorylation and its downstream signaling might have enhanced the levels of ER stress chaperones and apoptotic response, and inhibited global protein synthesis leading to the pathological conditions of the chagasic heart.

To evaluate the effect of cardiac ER stress and the downstream effect of P-eIF-2α signaling on the pathogenesis of cardiomyopathy in *T. cruzi* infected mice, we treated infected mice with 2AP, an inhibitor of P-eIF-2α after the acute infection (40 DPI) for 80 days and evaluated its effect on cardiac ER stress, mitochondrial stress and inflammation. A consequence of eIF-2α phosphorylation is upregulation of protein chaperons (Harding *et al*., 2000; B'chir *et al*., 2013; Volmer and Ron, 2015). 2AP inhibits eIF-2α phosphorylation and protein chaperons' upregulation, and prevents apoptosis, and induce protein synthesis, which are required for the normal functioning of the cells. Treatment of infected mice with 2AP significantly reduced ER stress by decreasing P-eIF2α levels and its downstream signaling. Inhibition of ER stress also significantly reduced cardiac inflammation, apoptosis and fibrosis, and improved contractile ability of the hearts during chronic

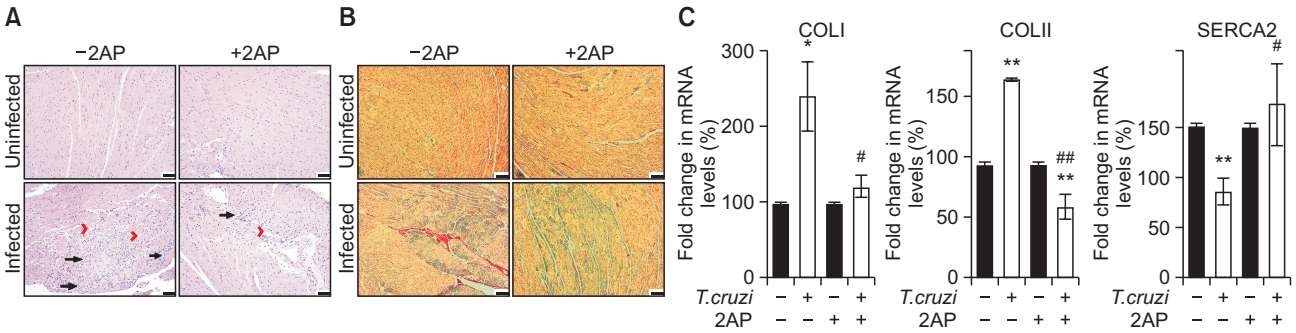

Fig. 6. Amelioration of cardiac pathology (inflammation, fibrosis, degenerating cardiac muscle fibre and accumulated lipid droplets) by 2AP in mice during chronic infection at 120 DPI (n=8, minimum five images/section were analyzed). (A) H&E staining displayed significantly more damage (inflammation – long black arrow, fibrosis – red arrow head, degenerating cardiac muscle fibre – black arrow head (See Supplementary Fig. 3) and presence of adipocytes or lipid granules – red long arrow (See Supplementary Fig. 3)) in infected mice hearts compared to the hearts of uninfected mice. However, infected 2AP treated mice displayed significantly reduced damage ($p \leq 0.01$) compared to infected untreated mice (bar –100 um). Additional images are presented as Supplementary Fig. 3. (B) The photomicrographs of trichrome Masson stained hearts sections demonstrated significant ($p \leq 0.01$) increase in cardiac fibrosis and collagen deposition in infected mice compared to uninfected mice. Infected 2AP treated mice showed significantly reduced damage ($p \leq 0.01$) compared to infected untreated mice (bar –100 um). (C) qPCR analysis demonstrated a significant increase in the cardiac mRNA levels of collagen I and III, and decrease in SERCA 2 in the infected mice compared to uninfected mice. Whereas, the mRNA levels of collagen I and III in infected 2AP treated mice were significantly reduced compared to infected untreated mice. Statistical significance compared to uninfected untreated mice and infected untreated mice are represented by $^{*}p \leq 0.05$, $^{***}p \leq 0.001$, and $^{\#}p \leq 0.05$ or $^{\#\#}p \leq 0.01$, respectively.

Chagas infection. More importantly, cardiac inhibition of ER stress significantly modulated ventricular enlargements commonly observed in murine chronic Chagas disease models.

Together, these results suggest that ER stress plays a major role in the pathogenesis of Chagas disease by elevating cardiac inflammation, apoptosis, and fibrosis during the long period of the indeterminate stage of infection. These changes promote heart pathology and elevate the risk of ventricular dilations of the heart in *T. cruzi* infected mice and, potentially, human CD patients.

In conclusion, this report demonstrated that ER stress occurred in the hearts of infected mice, as revealed by increased phosphorylation eIF-2α and increased expression of other ER chaperones. Our data provide clear evidence that chronic *T. cruzi* infection induced ER stress impairs cardiac ventricular internal diameters and an early treatment to reduce ER stress modulate/prevent the pathogenesis of cardiomyopathy in a murine Chagas model. A therapeutic strategy targeting cardiac ER stress inhibition during asymptomatic stage may be a valuable tool to combat development and progression of cardiomyopathy in Chagas patients.

CONFLICT OF INTEREST

None of the authors have conflict of interest.

ACKNOWLEDGMENTS

We thank Erika Shor at the Public Health Research Institute for a critical reading of the manuscript. This study was supported by grants from the National Heart, Lung, and Blood Institute (National Institutes of Health HL-122866) to Jyothi Nagajyothi.

REFERENCES

B'chir, W., Maurin, A. C., Carraro, V., Averous, J., Jousse, C., Muranishi, Y., Parry, L., Stepien, G., Fafournoux, P. and Bruhat, A. (2013) The eIF2α/ATF4 pathway is essential for stress-induced autophagy gene expression. *Nucleic Acids Res.* **41**, 7683-7699.

Cao, S. S. and Kaufman, R. J. (2014) Endoplasmic reticulum stress and oxidative stress in cell fate decision and human disease. *Antioxid. Redox Signal.* **21**, 396-413.

Carpio, M. A., Michaud, M., Zhou, W., Fisher, J. K., Walensky, L. D. and Katz, S. G. (2015) BCL-2 family member BOK promotes apoptosis in response to endoplasmic reticulum stress. *Proc. Natl. Acad. Sci. U.S.A.* **112**, 7201-7206.

Combs, T. P., Mukherjee, S., De Almeida, C. J., Jelicks, L. A., Schubert, W., Lin, Y., Jayabalan, D. S., Zhao, D., Braunstein, V. L., Landskroner-Eiger, S., Cordero, A., Factors, S. M., Weiss, L. M., Lisanti, M. P., Tanowitz, H. B. and Scherer, P. E. (2005) The adipocyte as an important target cell for Trypanosoma cruzi infection. *J. Biol. Chem.* **280**, 24085-24094.

Fernandas, O., Santos, S. S., Cupolillo, E., Mendonça, B., Derre, R., Junqueira, A. C. V., Santos, L. C., Sturm, N. R., Naiff, R. D., Barret, T. V. and Campbell, D. A. (2001) A mini-exon multiplex polymerase chain reaction to distinguish the major groups of *Trypanosoma cruzi* and *T. rangeli* in the Brazilian Amazon. *Trans. R. Soc. Trop. Med. Hyg.* **95**, 97-99.

Feng, C. Y. and Rise, M. L. (2010) Characterization and expression analyses of anti-apoptotic Bcl-2-like genes NR-13, Mcl-1, Bcl-X1 and Bcl-X2 in Atlantic cod (Gadus morhua). *Mol. Immunol.* **47**, 763-784.

Gardner, B. M., Pincus, D., Gotthardt, K., Gallagher, C. M. and Walter, P. (2013) Endoplasmic reticulum stress sensing in the unfolded protein response. *Cold Spring Harb. Perspect. Biol.* **5**, a013169.

Garg, N., Popov, V. L. and Papaconstantinou, J. (2003) Profiling gene transcription reveals a deficiency of mitochondrial oxidative phosphorylation in *Trypanosoma cruzi*-infected murine hearts: implications in chagasic myocarditis development. *Biochim. Biophys. Acta* **1638**, 106-120.

Gupta, S., Wen, J. J. and Garg, N. J. (2009) Oxidative stress in Chagas disease. *Interdiscip. Perspect. Infect. Dis.* **2009**, 190354.

Han, J. and Kaufman, R. J. (2016) The role of ER stress in lipid metabolism and lipotoxicity. *J. Lipid Res.* **57**, 1329-1338.

Harding, H.P., Zhang, Y., Bertolotti, A., Zeng, H. and Ron, D. (2000)

Perk is essential for translational regulation and cell survival during the unfolded protein response. *Mol. Cell* **5**, 897-904.
Jacquemyn, J., Cascalho, A. and Goodchild, R. E. (2017) The ins and outs of endoplasmic reticulum-controlled lipid biosynthesis. *EMBO Rep.* **18**, 1905-1921.
Jelicks, L. A. and Tanowitz, H. B. (2011) Advances in imaging of animal models of Chagas disease. *Adv. Parasitol.* **75**, 193-208.
Jelicks, L. A., Chandra, M., Shtutin, V., Tang, B., Christ, G. J., Factor, S. M., Wittner, M., Huang, H., Douglas, S. A., Weiss, L. M., Orleans-Juste P. D., Shirani J. and Tanowitz H. B. (2002) Phosphoramid on treatment improves the consequences of chagasic heart disease in mice. *Clin. Sci. (Lond.)* **103**, 267S-271S.
Johndrow, C., Nelson, R., Tanowitz, H., Weiss, L. M. and Nagajyothi, F. (2014) *Trypanosoma cruzi* infection results in an increase in intracellular cholesterol. *Microbes Infect.* **16**, 337-344.
Kezia, L., Janeesh, P. A., Cui, M. H., Rashmi B., Jelicks, L. A. and Nagajyothi, F. (2018) High fat diet aggravates cardiomyopathy in murine chronic Chagas disease. *Microbes Infect.* **18**, 1286-4579.
Li, X., Zhao, D., Guo, Z., Li, T., Qili, M., Xu, B., Qian, M., Liang, H., Xiaoqiang, E., Gitau, S. C., Wang, L., Huangfu, L., Wu, Q., Xu, C. and Shan, H. (2016) Overexpression of SerpinE2/protease nexin-1 contribute to pathological cardiac fibrosis via increasing collagen deposition. *Sci. Rep.* **6**, 37635.
Lipskaia, L., Chemaly, E. R., Hadri, L., Lompre, A. M. and Hajjar, R. J. (2010) Sarcoplasmic reticulum Ca2+ ATPase as a therapeutic target for heart failure. *Expert Opin. Biol. Ther.* **10**, 29-41.
Machado, F. S., Jelicks, L. A., Kirchhoff, L. V., Shirani, J., Nagajyothi, F., Mukherjee, S., Nelson, R., Coyle, C. M., Spray, D. C., de Carvalho, A. C., Guan, F., Prado, C. M., Lisanti, M. P., Weiss, L. M. Montgomery, S. P. and Tanowitz, H. B. (2012) Chagas heart disease: report on recent developments. *Cardiol. Rev.* **20**, 53-65.
Malhotra, J. D. and Kaufman, R. J. (2007) The endoplasmic reticulum and the unfolded protein response. *Semin. Cell Dev. Biol.* **18**, 716-731.
Memorial, C. C. (2009) Chagas disease and its toll on the heart. *Eur. Heart J.* **30**, 2063-2072.
Minning, T. A., Weatherly, D. B., Flibotte, S. and Tarleton, R. L. (2011) Widespread, focal copy number variations (CNV) and whole chromosome aneuploidies in Trypanosoma cruzi strains revealed by array comparative genomic hybridization. *BMC Genomics* **12**, 139-150.
Nagajyothi, F., Weiss, L. M., Zhao, D., Koba, W., Jelicks, L. A., Cui, M. H., Factor, S. M., Scherer, P. E. and Tanowitz, H. B. (2014) High fat diet modulates *Trypanosoma cruzi* infection associated myocarditis. *PLoS Negl. Trop. Dis.* **8**, e3118.
Nunes, M. C. P., Dones, W., Morillo, C. A., Encina, J. J. and Ribeiro, A. L. (2013) Chagas disease: an overview of clinical and epidemiological aspects. *J. Am. Coll. Cardiol.* **62**, 767-776.
Quijano-Hernandez, I. and Dumonteil, E. (2011) Advances and challenges towards a vaccine against Chagas disease. *Hum. Vaccin.* **7**, 1184-1191.
Rozpedek, W., Pytel, D., Mucha, B., Leszczynska, H., Diehl, J. A. and Majsterek, I. (2016) The role of the PERK/eIF2α/ATF4/CHOP signaling pathway in tumor progression during endoplasmic reticulum stress. *Curr. Mol. Med.* **16**, 533-544.
Soares, M. B. P., De Lima, R. S., Rocha, L. L., Vasconcelos, J. F., Rogatto, S. R., Dos Santos, R. R., Iacobas, S., Goldenberg, R. C., Iacobas, D. A., Tanowitz, H. B., de Carvalho, A. C. and Spray, D. C. (2010) Gene expression changes associated with myocarditis and fibrosis in hearts of mice with chronic chagasic cardiomyopathy. *J. Infect. Dis.* **202**, 416-426.
Tanowitz, H. B., Kirchhoff, L. V., Simon, D., Morris, S. A., Weiss, L. M. and Wittner, M. (1992) Chagas' disease. *Clin. Microbiol. Rev.* **5**, 400-419.
Tostes, S., Bertulucci, D., Pereira, G. and Rodrigues. V. (2005) Myocardiocyte apoptosis in heart failure in chronic Chagas' disease. *Int. J. Cardiol.* **99**, 233-237.
Van Kerckhoven, R., Kalkman, E. A., Saxena, P. R. and Schoemaker, R. G. (2000) Altered cardiac collagen and associated changes in diastolic function of infarcted rat hearts. *Cardiovasc. Res.* **46**, 316-323.
Volmer, R. and Ron, D. (2015) Lipid-dependent regulation of the unfolded protein response. *Curr. Opin. Cell Biol.* **33**, 67-73.
Weber, G. F. and Menko, A. S. (2005) The canonical intrinsic mitochondrial death pathway has a non-apoptotic role in signaling lens cell differentiation. *J. Biol. Chem.* **280**, 22135-22145.
Westphal, D., Dewson, G., Czabotar, P. E. and Kluck, R. M. (2011) Molecular biology of Bax and Bak activation and action. *Biochim. Biophys. Acta* **1813**, 521-531.
Zhao, L. and Ackerman, S. L. (2006) Endoplasmic reticulum stress in health and disease. *Curr. Opin. Cell Biol.* **18**, 444-452.
Zhou, L., Yang, D., Wu, D. F., Guo, Z. M., Okoro, E. and Yang, H. (2013) Inhibition of endoplasmic reticulum stress and atherosclerosis by 2-aminopurine in apolipoprotein e-deficient mice. *ISRN Pharmacol.* **2013**, 847310.